
The Early History of Reentry Physics Research at Lincoln Laboratory

Leo J. Sullivan

■ During the period from June 1958 through September 1965 Lincoln Laboratory engaged in a reentry measurements program that developed radar and optical instrumentation for observing the phenomena associated with the hypervelocity reentry of payloads into the earth's atmosphere. This article describes both the Lincoln Laboratory effort and the development and launching of reentry test vehicles by NASA.

IN 1953 THE SOVIET UNION exploded their first thermonuclear device, and the possibility of their joining that device with a long-range ballistic missile became a real threat for the United States [1]. Government and research facilities realized that this threat called for an increased research effort to study reentry phenomena. Discussions in 1958 with representatives of the then National Advisory Committee for Aeronautics (NACA), located at Langley Air Force Base, Va., revealed that NACA was designing a test vehicle to reenter small payloads into the earth's atmosphere at velocities in the neighborhood of 20,000 ft/sec. At the same time, Lincoln Laboratory, motivated by the threat posed by the Soviet Union's successful development of long-range ballistic missiles, became interested in the problem of warhead reentry and in the radar and optical phenomena associated with hypersonic reentry into the earth's atmosphere.

The importance of controlled experiments with known aerodynamic configurations to study reentry phenomena became obvious, and Lincoln Laboratory joined forces with NACA in a cooperative Reentry Physics Research Program. NACA, which became the National Aeronautics and Space Administration (NASA) on 1 October 1958, was responsible for the design and launch of reentry vehicles, and Lincoln Laboratory was responsible for the development and construction of the radar and optical instrumentation to observe the reentries, along with

the gathering and interpretation of data.

Foundations in Meteor Research

In 1958 the knowledge of the phenomena associated with the hypersonic entry of a body into the earth's atmosphere had been obtained only by observing natural meteors. By using optical and radar techniques, meteor astronomers had accumulated considerable knowledge of the effects produced by meteors interacting with the earth's atmosphere. The earliest radar observations of meteors had been made at long wavelengths (approximately 30 MHz) by using both pulsed and continuous-wave transmissions. At that frequency only the meteor trail could be seen. Later, because of increased power generation capability at higher frequencies, the signals reflected from the ionized region in the immediate vicinity of the meteor were observed at 200 MHz and above.

The production of an ionized trail by meteors was well known, and the degree of ionization in the trail (whether it was underdense or overdense) was well understood. At frequencies of 200 MHz and greater, so-called *head echoes*, or radar reflections from the ionized plasma in front of the reentry body, were observed. The head echoes traveled at the same speed as the meteor, and the combination of the Doppler frequency and the range-versus-time data of the head echo provided a direct measure of meteor velocity.

Results of meteor research led to the following con-

clusions: (1) radar returns are obtained from the ionized trail, or wake, produced by a reentry body, (2) radar backscattering from the ionized bow shock, or region in the immediate vicinity in front of the reentry body, is observed, and (3) the critical frequencies for radar measurements of a reentry body are found in the microwave region between UHF (400 MHz) and X-band (10 GHz).

Radar Instrumentation

On the basis of the results of meteor research we decided that radar observations of a reentry body should be made at three different frequencies throughout the complete trajectory. The frequencies selected were UHF (400 MHz), S-band (3 GHz), and X-band (10 GHz). We further decided that the rocket vehicle should be automatically tracked in angle and range by radar, starting immediately after launch and going through all stage separations, including reentry, without the aid of any radiating device such as a beacon or transponder in the vehicle. We selected the S-band frequency of 3 GHz as

the operating frequency for the angle-tracking system. The UHF and X-band frequencies, along with the S-band, were used to measure the cross sections of the bow shock and turbulent wake of the reentry body.

The reentry body was a 5-in sphere with an S-band cross section of 0.01 m^2 . Tracking a reentry body of this size out to a range of 200 nmi imposed a demanding requirement on the tracking radar. This tracking requirement, along with limited component availability, essentially determined the design of the S-band angle-tracking radar.

Because of time pressures on the program, we decided to use an existing 60-ft parabolic antenna mounted on a surplus U.S. Navy Dual 5-in/38-caliber gun mount (see Figure 1). The most powerful S-band transmitter available at that time was the transmitter used with the Air Force FPS-6 height-finding radar. The magnetron in this transmitter developed a peak output of approximately 4.5 MW at a pulse width of $2 \mu\text{sec}$, which represented a good compromise between range



FIGURE 1. Radar antennas at the Lincoln Laboratory field site at Arbutle Neck, Va., located near the NASA Wallops Island launch facility. Site instrumentation consists of (from right to left) the S-band tracking radar, the multiplexed UHF and X-band cross-section measurements radar, and the SPANDAR long-range trajectory and range-safety radar designed by Lincoln Laboratory for NASA.

resolution and sensitivity.

In spite of the advantages of four-horn monopulse for angle tracking and signal-amplitude measurement, conical-scan angle tracking was selected because a low-noise receiver was needed to insure a signal-to-noise ratio adequate for tracking the small target at maximum range. The state of the art in receiver design at the time was such that low-noise amplification using a maser or parametric amplifier was feasible only in a conical scan receiver that required only a single channel. The phase and amplitude stability of three separate RF channels with parametric amplification, which was required by a monopulse system, had not been demonstrated at that time. Accordingly, we decided to use conical-scan angle tracking with a nitrogen-cooled parametric amplifier that was designed and built at Lincoln Laboratory. Later, when the phase stability of cooled parametric amplifiers had progressed sufficiently, the target angle-tracking subsystem was modified to a four-horn amplitude monopulse configuration.

We decided that the UHF and X-band radars should be diplexed in a second available 60-ft antenna that was also mounted on a Navy 5-in/38-caliber gun mount; this diplexed radar was then slaved to the S-band tracker (Figure 1). Lincoln Laboratory had previously developed high-powered UHF transmitters and modulators in support of the Boston Hill search radar, which was a prototype for the Air Force FPS-35 search radar. The VA 812C series UHF klystron, which was capable of a power output of approximately 8 MW at the pulse widths and pulse repetition rates of interest, was selected as the transmitter tube for the UHF radar, and a transmitter unit and modulator essentially identical with the Boston Hill system was procured. The scattering cross sections of the ionized wake and flow field were not well known at the time. We knew that the cross sections were low, but at the same time we recognized the advantages of range resolution. The alternating transmission of pulses that were 6 μ sec and 1 μ sec in duration was chosen to give both maximum pulse energy (to measure the cross sections) and accurate range resolution.

The UHF transmitter consisted of a power amplifier chain excited by a stable continuous-wave source, but the limited availability of resources initially led to the use of simple amplitude detection, which did not take advantage of the coherent capability inherent in the UHF

transmitter system. The UHF receiver system was later modified by the addition of a coherent signal processing and recording system. A square-horn UHF feed allowed both vertical and horizontal polarization. Transmission was at the vertical polarization, with simultaneous reception of both the vertically and horizontally polarized backscattered components. The UHF feed illuminated the full 60-ft aperture of the antenna.

The X-band cross-section measurement system utilized the same reflector as the UHF cross-section measurement system. Because of the narrow beamwidth produced by a fully illuminated 60-ft reflector at X-band, the rectangular X-band horn located in the center of the UHF horn was restricted to illuminating only an elliptical area approximately 20 ft \times 15 ft. By illuminating a smaller area of the antenna we increased the width of the X-band beam, which kept the target body more easily within the beam. We utilized the highest-power X-band transmitting tube available at that time, which consisted of a magnetron with a peak power of approximately 1 MW at a pulse width of 2 μ sec.

A low-noise front-end preamplifier was essential to maximize the sensitivity of the receiver. At the time, because of the lack of a parametric X-band preamplifier, a maser was the only choice as a low-noise preamplifier. Accordingly, Lincoln Laboratory designed and built the world's first X-band maser preamplifier and installed it in the X-band radar at Arbuckle Neck, Va.

Installation of Radar Instrumentation

The NASA head start in designing and building a launch vehicle forced the radar instrumentation program at Lincoln Laboratory into a tail chase from the beginning. Trailblazer I α was launched by NASA on 3 March 1959 and Trailblazer I β was launched on 4 June 1959. Both of these launches occurred without any radar coverage at all and with optical instrumentation consisting only of surplus K-2 aerial ballistic cameras with rotating choppers to provide a time base. No spectral coverage existed at the time.

The S-band tracking radar built at Lincoln Laboratory and tested at Millstone Hill became operational at Arbuckle Neck in time for the 1 December 1959 launch of the Trailblazer I γ vehicle from Wallops Island. The S-band radar acquired the rocket vehicle after launch, during the early up-firing stage burning, and switched



FIGURE 2. The 60-ft antenna and mount of the SPANDAR S-band tracking radar designed by Lincoln Laboratory for NASA.

track at each stage separation, including the 5-in spherical rocket-body sixth stage. The radar continued to track throughout reentry. The installation of the UHF and X-band measurement systems at Arbutle Neck soon followed the launch of Trailblazer I γ , and the completely integrated multiwavelength measurement system became operational.

The SPANDAR Radar

Concurrently with the design and construction of the initial S-band tracking radar and the X-band and UHF radar mentioned above, Lincoln Laboratory developed a second high-power S-band tracking radar, the Space Range Radar (SPANDAR), for NASA and installed it at the Lincoln Laboratory field site at Arbutle Neck (Figure

2). This radar used a 60-ft paraboloidal antenna with a conical-scan feed identical to that on the S-band tracking radar. It was mounted on a Millstone Hill radar antenna mount instead of a surplus Navy gun mount like those used for the other Lincoln Laboratory radars. Even though the transmitting and receiving systems of the SPANDAR radar resembled those of the S-band tracking radar, its design and operating parameters were intended for long-range tracking of satellites and rocket vehicles in both the multiple-pulse beacon transmitter mode and the skin-tracking mode.

Radar Data Collection and Processing

The Arbutle Neck radar system was one of the first systems to be specifically designed as an integrated multiple-frequency cross-section measurement system. Figure 3 is a photograph of the integrated measurement system as it looked after installation in 1959. From the beginning of the program the guiding principle was that the radar complex should be designed as a complete data-gathering and processing system with the data gathering performed at Arbutle Neck (which was on the Virginia mainland west of the Wallops Island launch site) and all data processing and analysis performed at Lincoln Laboratory in Lexington, Mass.

Direct digital recording on magnetic tape was selected as the primary method for recording all radar signals. The signals at the three radar frequencies (and for both polarizations of the UHF radar) were simultaneously time-gated with range gates, and the peak value reached during the gating interval was digitized and recorded on magnetic tape. The time, azimuth, elevation, and range already existed in digital form and were recorded simultaneously with the signal data. The original digital system recorded each parameter on separate tape tracks. This integrated digital measurement system was the first highly capable digital data-recording system in the country.

After a launch, the data tape was transported to Lexington, where it was read into the IBM 704 at the central computer facility. During the period of the reentry program, the 704 was successively superseded by the 709, the 7090, and finally the 7094. Because the data tape was not in IBM format, translation equipment—the so-called Codal translator—was required to play back the digital data into the real time input of the 704 and its successors.

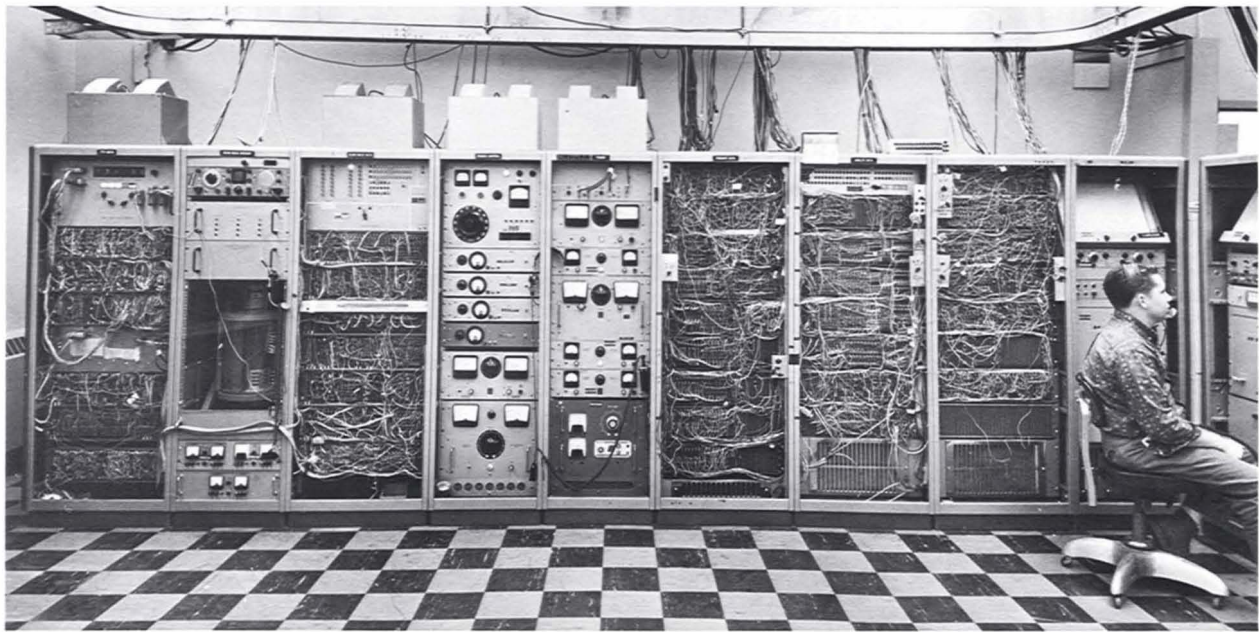


FIGURE 3. The integrated multiple-frequency cross-section measurement and recording system. This system was the first highly capable digital data-recording system in the country.

Because the digital system measured and recorded signal amplitude at only one range station, it was quickly supplemented by oscilloscope film recording that was designed to record over a range interval extending in front of and behind the tracked target. Film traces of multiple or extended targets could be examined visually for qualitative analysis, and trace deflections could be read manually to obtain preliminary quantitative results.

Manual film reading was a slow and laborious process, however, so an automatic film reader was designed and constructed. This reader consisted of a precision small-screen cathode ray tube whose spot focused on the moving film and scanned in a direction perpendicular to the recorded trace under the command of a PDP-1 digital computer. The displacements of the scanned spot were digitized and recorded as a measure of the amplitude versus time of the analog video signal originally recorded by the oscilloscope.

Optical Measurements

The production of optical radiation by meteors entering the earth's atmosphere was well known, and wide field-of-view optical measurement techniques and instrumentation to record meteor activity had reached a highly developed state. Meteor cameras had undergone an evolution from the early $f/6.3$ meteor patrol cameras built in

the thirties to the highly sensitive Super Schmidt cameras designed by James Baker and built in the 1940s by the Perkin-Elmer Corporation. The Super Schmidt cameras had a corrected field of view of approximately 55° and a geometric f number of 0.84, which made them extremely fast and useful for meteor photography. Spectrographic measurements were made by placing a dispersing element, such as a prism or grating, over the aperture. Although astronomers had photographed thousands of natural meteor trails, they had recorded only a few meteor spectra up to 1932, primarily because of the lower sensitivity due to the dispersion of the spectrographic camera. Interest in meteor spectra substantially increased after 1932, because of the increased performance of camera equipment and the development of higher-speed films, and by 1958 approximately 300 spectra were available.

In 1958 four Super Schmidt meteor trail cameras were in the possession of Harvard Observatory, which, in conjunction with the Smithsonian Astrophysical Observatory in Cambridge, Mass., was the world's leading center for meteor research. Because of this fact we decided that cooperation with Harvard Observatory would be fruitful, so we initiated a contract for the installation of two of Harvard's Super Schmidt cameras at the Lincoln Laboratory field site at Arbuckle Neck and the assistance

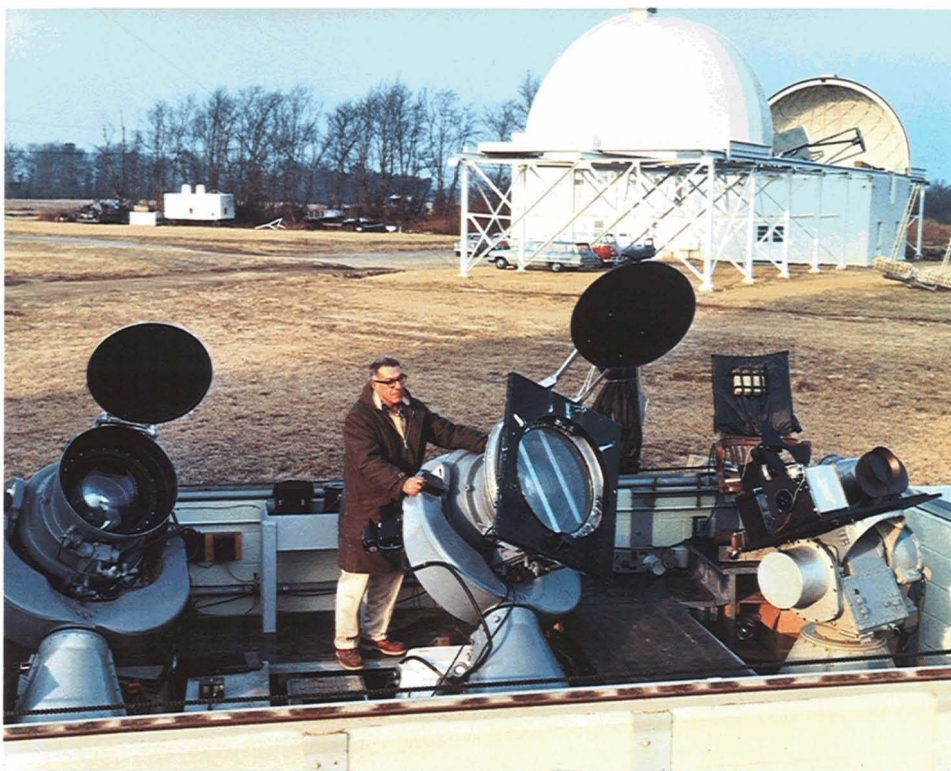


FIGURE 4. Optical instrumentation at the Lincoln Laboratory field site at Arbuckle Neck. At the left is one of the Harvard Observatory Super Schmidt cameras; in the middle is an identical Super Schmidt camera converted to a spectrograph by a triple-element Fresnel prism mounted in front of the camera aperture. The smaller Baby Schmidt camera at the far right, equipped with a grating, functions as a slitless spectrograph. The operator is Lawrence Prugnarola.

of Harvard Observatory staff in film processing, film reading, and data reduction. One of the Super Schmidt cameras was turned into a spectrograph by mounting a three-element plastic prism in front of the camera aperture. Both Super Schmidt cameras were equatorially mounted and were driven at the sidereal rate.

Because the performance of the Super Schmidt spectrograph was poor in the ultraviolet region, it was supplemented by the so-called Baby Schmidt camera, which was designed and built by the Perkin-Elmer Corporation to Lincoln Laboratory specifications. This smaller $f/0.83$ Schmidt camera had a 6-in aperture and a 20° field of view. Its corrector plate was fabricated from sagged Vicor glass whose optical transmission extended below 3000 \AA . Another small Schmidt camera owned by Harvard Observatory, the Paul Schmidt (named after the amateur astronomer who built it), was used with film sensitive in the near infrared to extend the wavelength coverage into that region. The Baby Schmidt camera and the Paul

Schmidt camera, because of their small field of view compared to the azimuth dispersion of the reentry event, were mounted on a single servo-driven two-axis altitude-azimuth mount slaved to the S-band tracking radar. The two cameras operated in track mode on this mount until shortly before the time of the reentry event; at that time the mount position was frozen and the cameras operated in trail mode. Figure 4 shows the two Super Schmidt cameras, along with the Baby Schmidt and the Paul Schmidt cameras, installed at the Arbuckle Neck site.

Simultaneous optical observations from two separated stations are required to determine the path and velocity of a reentry object. A second Super Schmidt camera station was therefore located at Eastville, Va., southwest of the Wallops Island launch site. This second camera position provided the required second observation of the reentry event. An ideal site for the second camera station was actually located farther south along the North Carolina coast; this ideal second site had a vantage point that

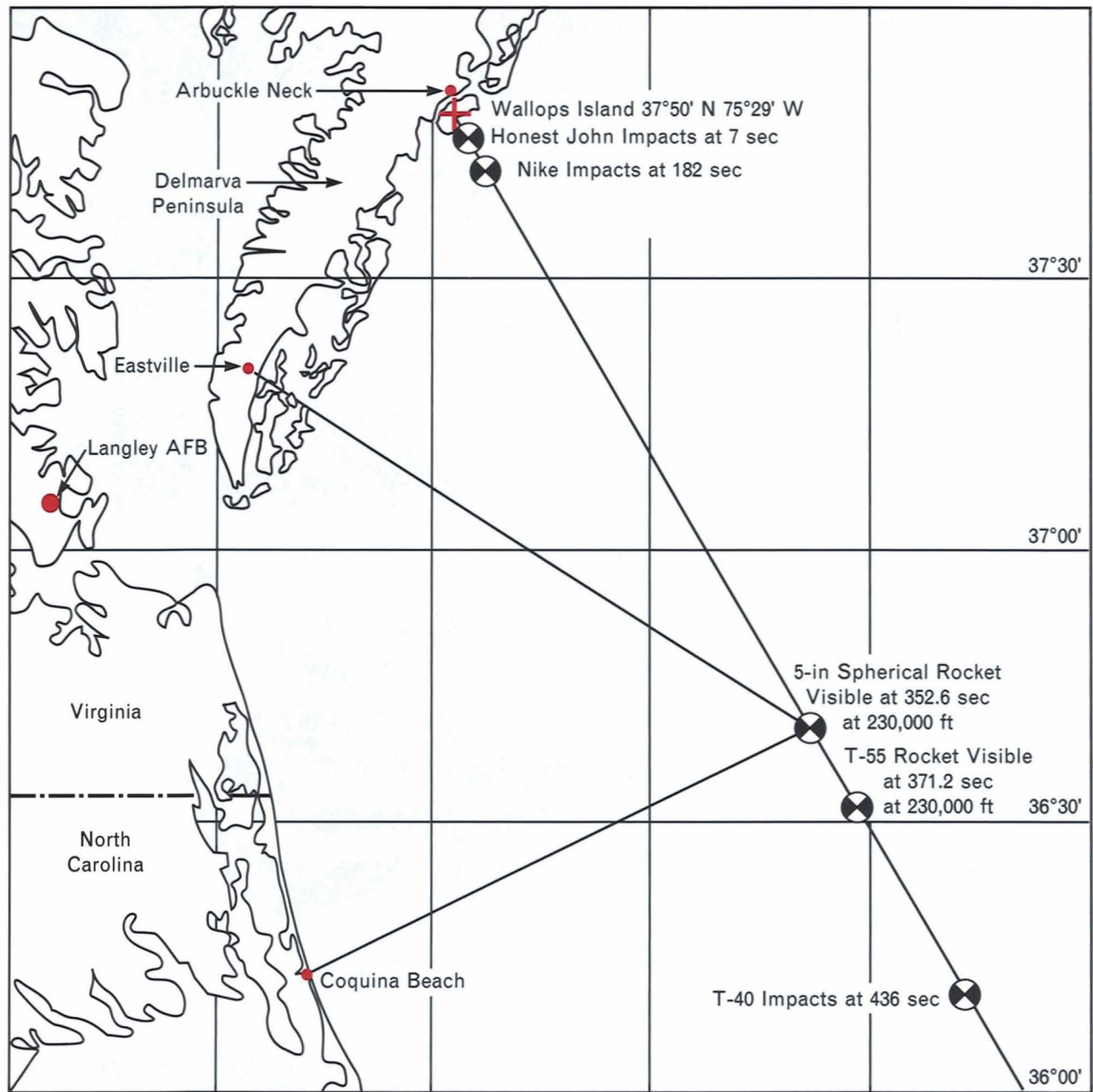


FIGURE 5. Map of the Delmarva Peninsula and the Virginia and North Carolina coastline regions, and the offshore impact regions of the Trailblazer launch vehicles. The NASA launch facility was located at Wallops Island, and the Lincoln Laboratory field site was located on the mainland at Arbutle Neck, Va. A second camera position at Eastville, Va., provided the necessary additional optical measurements of the reentering object.

could have provided minimum range, high elevation angle, and long baseline. The early beginnings of the Wallops Island program, however, took place before construction was completed on the bridge-tunnel connecting the southern tip of the Delmarva peninsula with Virginia and North Carolina, thus making travel to an ideal coastline observation point difficult. The travel

distance and the shortage of manpower led to the decision to confine our optical measurement activities initially to the Delmarva Peninsula near Wallops Island, even though it was measurably poorer for optical observations. Accordingly, the second Super Schmidt camera station was located at Eastville, Va. Additional cameras were later installed at Coquina Beach, N.C. Figure 5

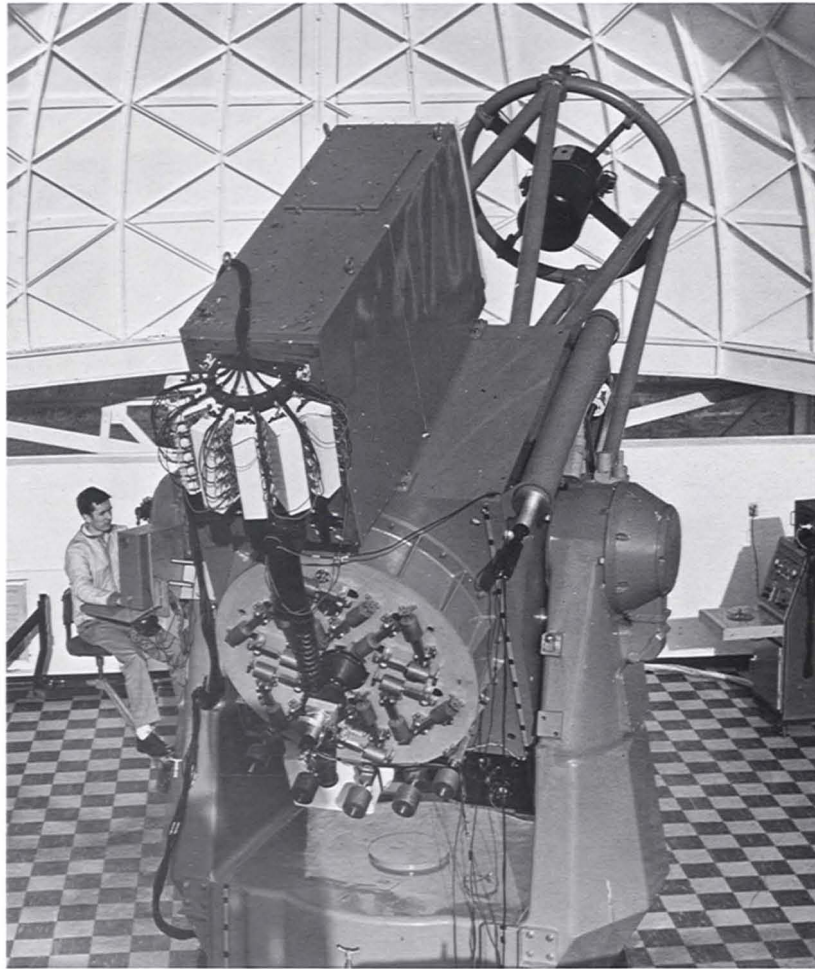


FIGURE 6. The 1.2-m Cassegrain telescope with the dual-wavelength spectrometer mounted on top. The spectrometer subdivided and measured the energy in the infrared region from 0.6 to 4.0 μm and in the visible region from 0.3 to 0.6 μm . The operator is James Daley.

illustrates the geography of the area around the Wallops Island launch site, along with the second camera locations and the impact regions of the launch vehicles.

Tracking Spectrometer

Early in the program we recognized the limitations placed on the optical observations by the low sensitivity of the wide field-of-view meteor cameras. We decided to design and build a narrow field-of-view tracking spectrometer that could either be slaved to the S-band tracking radar or operated autonomously by automatically angle-tracking the self-luminous plasma immediately adjacent to the reentry body.

A 1.2-m-aperture Cassegrain telescope configuration was selected for the light collector. This telescope consist-

ed of an $f/5$ paraboloidal primary mirror and a 16-in-diameter hyperboloidal secondary mirror that was mounted on a tip/tilt mechanism to provide the wideband vernier tracking loop required to track the high angular rates and accelerations of the reentry object. The overall f number of this telescope was $f/15$. The telescope was mounted on a high-precision azimuth/elevation mount powered by gearless torque motor drives; inductosyns were used for angular position measurement of the mount. The analog angle outputs were digitized and used for data recording and transmission.

The converging beam reflected by the secondary mirror passed through a hole in the primary mirror toward a focus at the angle-error sensor that operated in the visible spectral region. A beam splitter placed before the focus of

the telescope reflected part of the received energy to a lithium-fluoride prism. The prism separated the energy into two spectral bands—the visible from 0.3 to 0.6 μm and the infrared from 0.6 to 4.0 μm —and dispersed and imaged the infrared energy on 10 contiguous PbS detectors whose outputs were digitally recorded on magnetic tape. The visible energy was directed into a Czerny-Turner grating spectrometer equipped with 30 photon-counting photomultipliers that were cooled by circulating liquid freon. The outputs of the individual photomultipliers were then counted, cyclically scanned, digitized, and recorded on magnetic tape. Figure 6 shows the 1.2-m Cassegrain telescope with the spectrometer mounted above it.

The spectrometric telescope system was completed in 1963 near the end of the reentry measurements program. It was the most highly developed system of its kind at the time, and it successfully recorded visible spectrometric data on the last launch of the program.

The Development of the Trailblazer I Launch Vehicle

The reentry test vehicle designed by NASA was designated Trailblazer I. Figure 7 shows a Trailblazer I vehicle on the launcher at the NASA Wallops Island launch facility. The vehicle consisted of a six-stage solid-propellant rocket configuration in which the first three stages—the Honest John, Nike, and XM45 rockets—were successively fired to loft the *velocity package*, consisting of a nose shell containing three down-firing stages, to an altitude of approximately 1 million ft, or 200 mi. The down-firing motors were the T40, the T55, and the 5-in spherical motor. Figure 8 illustrates the configuration of the Trailblazer I launch vehicle and the velocity package, and Figure 9 shows a typical trajectory for a Trailblazer I launch.

The last down-firing stage reached a velocity of approximately 20,000 ft/sec, which is necessary to simulate realistically the phenomena generated by the reentry of an ICBM payload. This velocity requirement, along with the impulse limitations of each of the down-firing stages, imposed an upper limit of two pounds on the weight of the last stage, which in turn required that the last-stage rocket motor casing become the reentry body at motor burnout, and also required that the total impulse-to-motor-casing weight ratio be maximized.

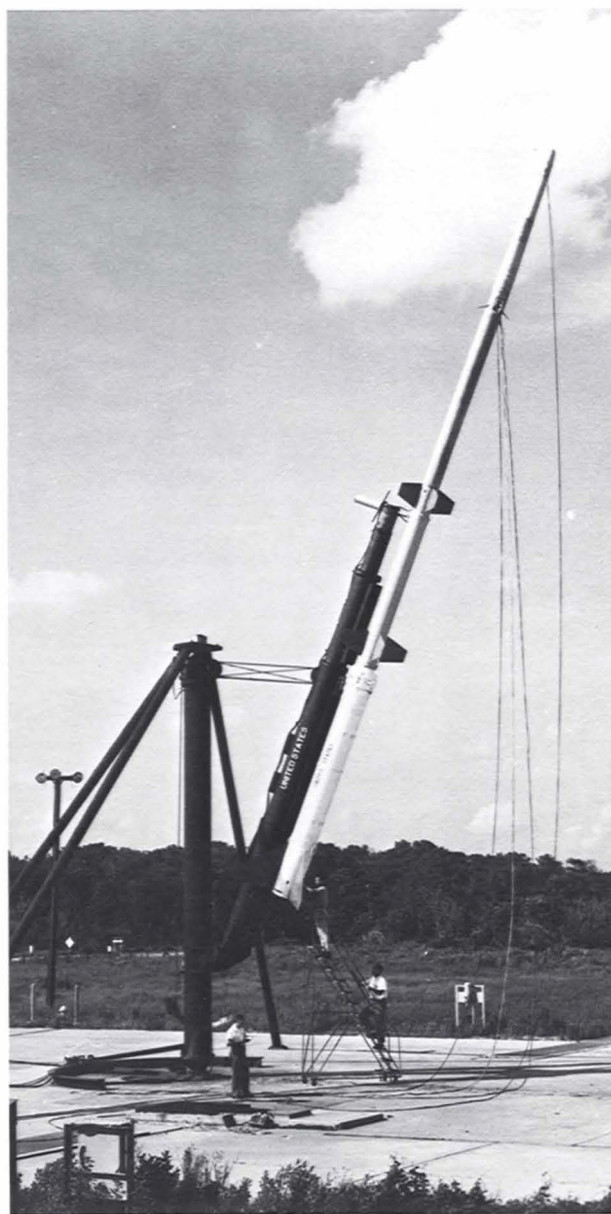
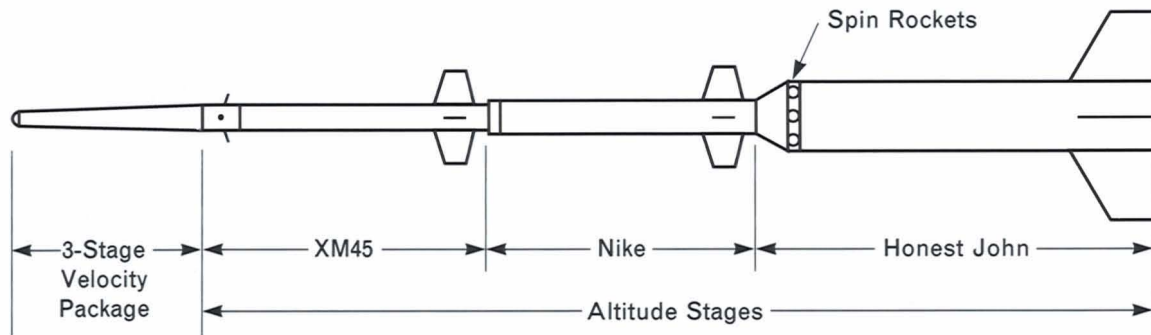
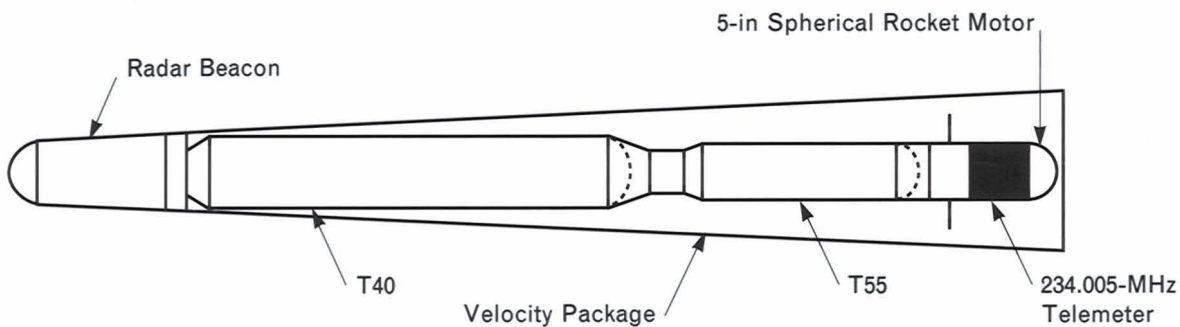


FIGURE 7. The six-stage Trailblazer I reentry vehicle on the launcher at the NASA Wallops Island launch facility. The entire launch vehicle, which was approximately 55 ft long, launched the velocity package to a height of approximately 200 mi. The three-stage down-firing velocity package reached a final velocity of 20,000 ft/sec.

A spherical motor, which is the optimum configuration for withstanding the high internal pressures generated by the burning propellant, was chosen as the sixth-stage, or reentry-stage, motor for the Trailblazer I rocket vehicles. To generate and radiate a continuous-wave signal at the 200-MHz frequency needed to measure Doppler velocity, NASA mounted a cylindri-



(a)



(b)

FIGURE 8. The overall configuration of the Trailblazer I launch vehicle and the velocity package containing the three down-firing stages. (a) The first three stages were Honest John, Nike, and XM45 rockets, and (b) the second three stages, the down-firing stages, were T40, T55, and 5-in spherical rockets.

cal metallic housing containing a transistorized transmitter on the front of the spherical-rocket-motor reentry body. The cylinder was insulated from the sphere and formed one half of a dipole that, along with the sphere, radiated in a toroidal radiation pattern. Figure 10 shows the configuration of the Trailblazer I reentry body with the cylindrical housing mounted on the front of the spherical rocket motor. The first two Trailblazer launches, designated Trailblazer I α and Trailblazer I β , used this reentry configuration. The signal from the reentry-body transmitter provided a measure of Doppler velocity. We soon recognized, however, that the blunt end of the cylinder (which was in contact with the hypersonic shock wave and was immediately followed by the ionized stagnation region) would severely influence the radar backscattering characteristics of those regions and would also substantially complicate the interpretation of the data on the backscat-

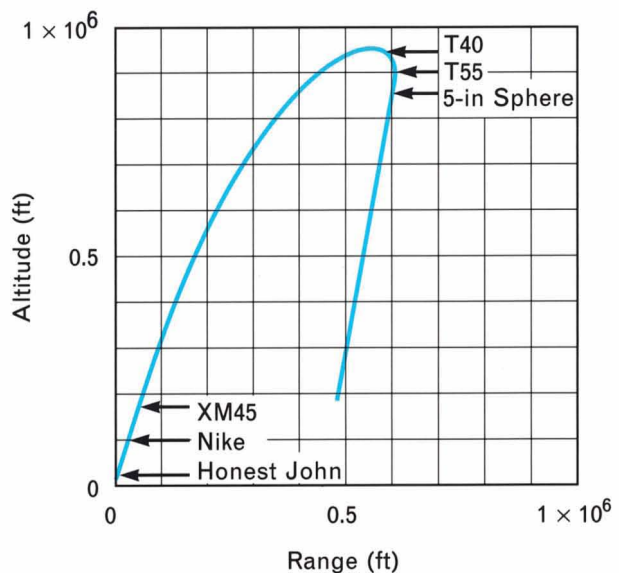


FIGURE 9. The staging sequence and trajectory for the Trailblazer I vehicle.

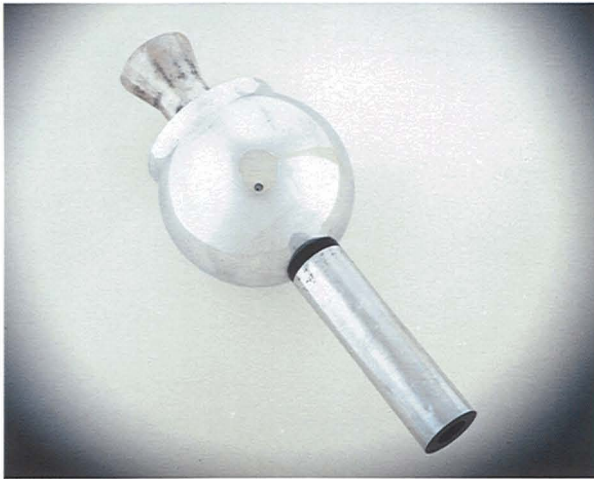


FIGURE 10. Early Trailblazer I reentry-body configuration with a continuous-wave transmitter and antenna mounted on front of the 5-in spherical motor. This configuration was used on the first two Trailblazer I launches.

tering from the ionized wake.

The arrival and installation of the Lincoln Laboratory S-band tracking radar eliminated the need for the NASA-installed continuous-wave beacon on the reentry body. Deleting the beacon placed the spherical reentry body in contact with the shock wave; this change simplified our measurements because the hypersonic flow characteristics of a spherical reentry body were better understood and described by aerodynamic theory at that time. The continuous-wave telemetry signal was then radiated by a dipole antenna in which the original cylindrical housing was replaced by an annular metallic cylinder containing the transmitter components. The annular cylinder was attached to the aft end of the reentry body, where it surrounded the nozzle. An insulating ring electrically isolated it from the motor body, with which it formed a dipole radiator. Figure 11 shows the modified configuration for the Trailblazer I reentry body; succeeding Trailblazer I reentry payloads beginning with Trailblazer I_y and Trailblazer I_a through Trailblazer I_j had this configuration. Table 1 summarizes the detailed characteristics of the Trailblazer launch vehicles along with their firing dates and reentry-body weights.

Development of the Trailblazer II Launch Vehicle

While experiments utilizing the Trailblazer I launch vehicles progressed, we realized that the two-pound maxi-

imum payload weight necessary to achieve a 20,000 ft/sec reentry velocity imposed a severe limitation on the configuration of the reentry object, which prevented a realistic simulation of many real-world scenarios. We decided accordingly that NASA would design a new four-stage rocket vehicle—designated Trailblazer II—with the capability of propelling a 35-pound reentry object to a velocity of 20,000 ft/sec. Figure 12 is a photograph of the Trailblazer II launch vehicle, and Figure 13 illustrates the configuration of the launch vehicle and the reentry stage. This new vehicle allowed more realistic reentry payload configurations and also allowed the installation of telemetry sensors in the reentry body. Figure 14 shows a typical Trailblazer II trajectory. Trailblazer II firings commenced in 1963 shortly after the completion of the Trailblazer I series of launches.

Summary of Trailblazer Reentry Results

At the start of the Trailblazer program, little was known about the electromagnetic scattering created by the ionized shock layer and turbulent wake generated by a hypervelocity vehicle reentering the atmosphere. The strong radar signals observed at S-band and UHF in the early Trailblazer reentries, even when viewed at an angle broadside to the wake, led to the hypothesis that the



FIGURE 11. Later Trailblazer I reentry-body configuration with the annular transmitter housing and antenna mounted aft of the spherical motor, surrounding the motor nozzle. Deleting the transmitter from the original configuration in front of the spherical reentry body placed the body directly in contact with the shock wave.

Table 1. Trailblazer I Launch Vehicle Characteristics

<i>Trailblazer Model No.</i>	<i>Date Fired</i>	<i>Reentering Configuration</i>	<i>Reentry Weight (lbs)</i>
I α	3 March 1959	Thin-Wall Aluminum Case with Spike Telemeter	0.77
I β	4 June 1959	Thin-Wall Aluminum Case with Spike Telemeter	0.80
I γ	1 December 1959	Heavy-Wall Titanium Case with Torus Telemeter	2.06
Ia	29 March 1960	Heavy-Wall Steel Case with Torus Telemeter	2.28
Ib	26 June 1960	Heavy-Wall Aluminum Case with Torus Telemeter	2.15
Ic	28 August 1960	Heavy-Wall Titanium Case with Torus Telemeter	2.10
Id	29 August 1960	Aluminum Case with Phenolic Nylon, Torus Telemeter	2.17
Ie	21 October 1960	Heavy-Wall Steel Case with Torus Telemeter	2.30
If	17 January 1961	Aluminum Case with Copper Shield, Torus Telemeter	1.99
Ig	21 April 1961	7th-Stage 2-g Steel Pellet in Aluminum Case	0.57
Ih	18 May 1961	Steel "J" Case with Dummy Torus Telemeter	1.56
Ii	16 September 1961	Aluminum Case (Thick Wall) with Dummy Torus Telemeter	1.41
Ij	2 April 1962	Aluminum Case, Ablating Phenolic Nylon, Dummy Torus Telemeter	1.53
Ik	27 July 1962	8-in Aluminum Case	2.00

major scattered signals came from a turbulent wake rather than any laminar shock layer or near-wake region. The Trailblazer I reentry vehicle was essentially a sphere, and this shape removed questions about effects due to angle of attack and aspect angle. The range extension of the returned radar pulses demonstrated that the scattering target indeed was extended in space behind the spherical reentry body. A statistical analysis of the amplitude of the returns from the trailing portions of the time-stretched pulses showed that the signals were essentially Rayleigh-

distributed. This analysis demonstrated that the signal was scattered from an ensemble of multiple scatterers, as would be expected in scattering from an ionized turbulent region.

Further evidence of the random or noisy character of the signal scattered from the wake was found in the first attempts to measure the deceleration of the reentry body more precisely by utilizing the phase information obtained from the coherent UHF radar. Although the low repetition rate of the UHF radar resulted in velocity

ambiguities, these ambiguities could be resolved and the phase progression in the signal from the single hard target could be followed until scattering from the wake was observed. At the point when the wake was observed, the phase information became noisy, and the velocity ambiguities could no longer be resolved because of the low repetition rate of the radar.

Evidence that the major portion of the energy scattered from the wake came from low-velocity regions was first obtained by the Millstone Hill Radar (located in Westford, Mass.) observations of Trailblazer I reentries. The Millstone Hill Radar had poor range resolution but good Doppler resolution, and the data showed that most of the scattered energy during reentry appeared near zero Doppler. Thus we concluded that the major portion of the wake was traveling at low velocities. The pulse width of the UHF radar at Arbutle Neck was then shortened to $0.25 \mu\text{sec}$ to increase the range resolution, and the repetition rate was increased to 960 pulses per second to reduce the ambiguity problem. The data recorded following this modification helped to confirm the earlier evidence of low velocities in the wake.

The first observations of high-altitude initial shock-layer formation and of the cross-section dip at or near-initial shock formation were made in the Trailblazer I experiments. Figure 15 shows the UHF cross section versus altitude for a Trailblazer I launch on 27 July 1962; the dip in cross section clearly occurs at a height of approximately 250,000 ft. Because the reentry bodies were spherical, no variation in cross section resulted from changes in the aspect angle; with a more complex object the changes in aspect angle would mask the effects of plasma formation. The Trailblazer I experiments with spherical reentry bodies, such as the object illustrated in Figure 16, strongly influenced the similar Bell Laboratory experiments in the early 1960s. In these experiments spheres were flown as secondary payloads along with reentry measurement vehicles launched from Vandenberg Air Force Base located in California into the Kieran Reentry Measurements Site (KREMS) located on Roi-Namur Island in the Marshall Islands Group in the western Pacific Ocean.

The study of the radar pulse shapes prior to the appearance of the large wake return frequently revealed the appearance of apparent wake instabilities that increased in amplitude and eventually produced the large

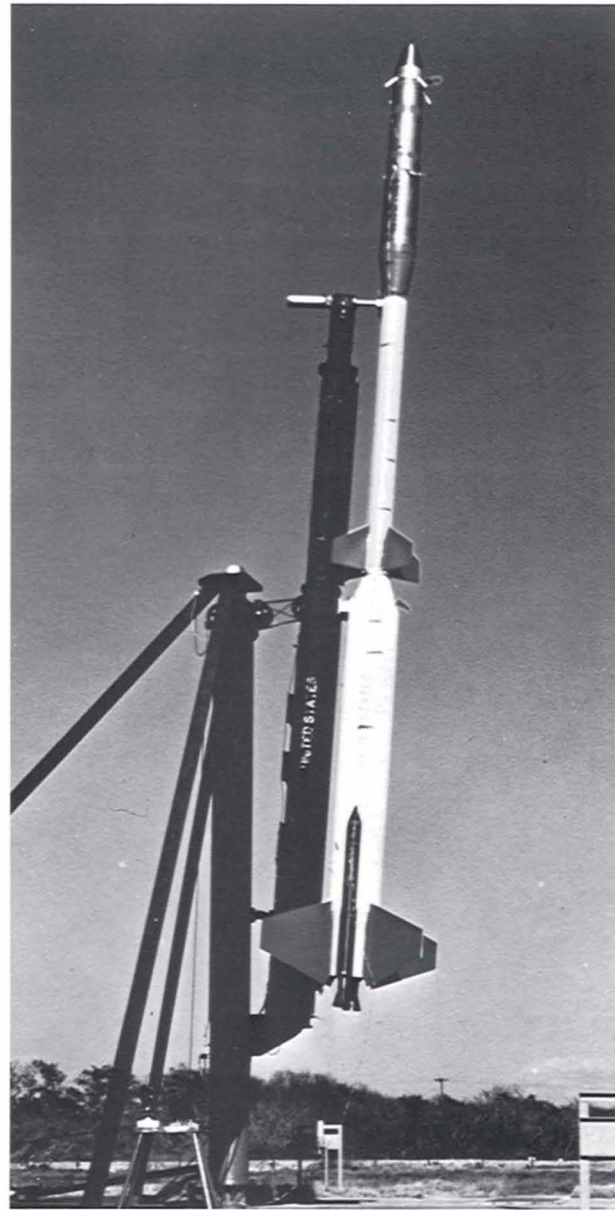


FIGURE 12. Trailblazer II four-stage reentry vehicle on the launcher at the NASA Wallops Island launch facility.

wake return. A detailed pulse-by-pulse examination of the formation of the wake return showed that the wake return first appeared at some distance behind the reentry body, increased in magnitude, and moved toward the reentry body as it descended in altitude. Measurements of the distance from the body to the beginning of the wake return at high altitude on some of the reentries showed close agreement with the prediction of transition distance from scaled hypervelocity ballistic-range measurements on subscale reentry objects.

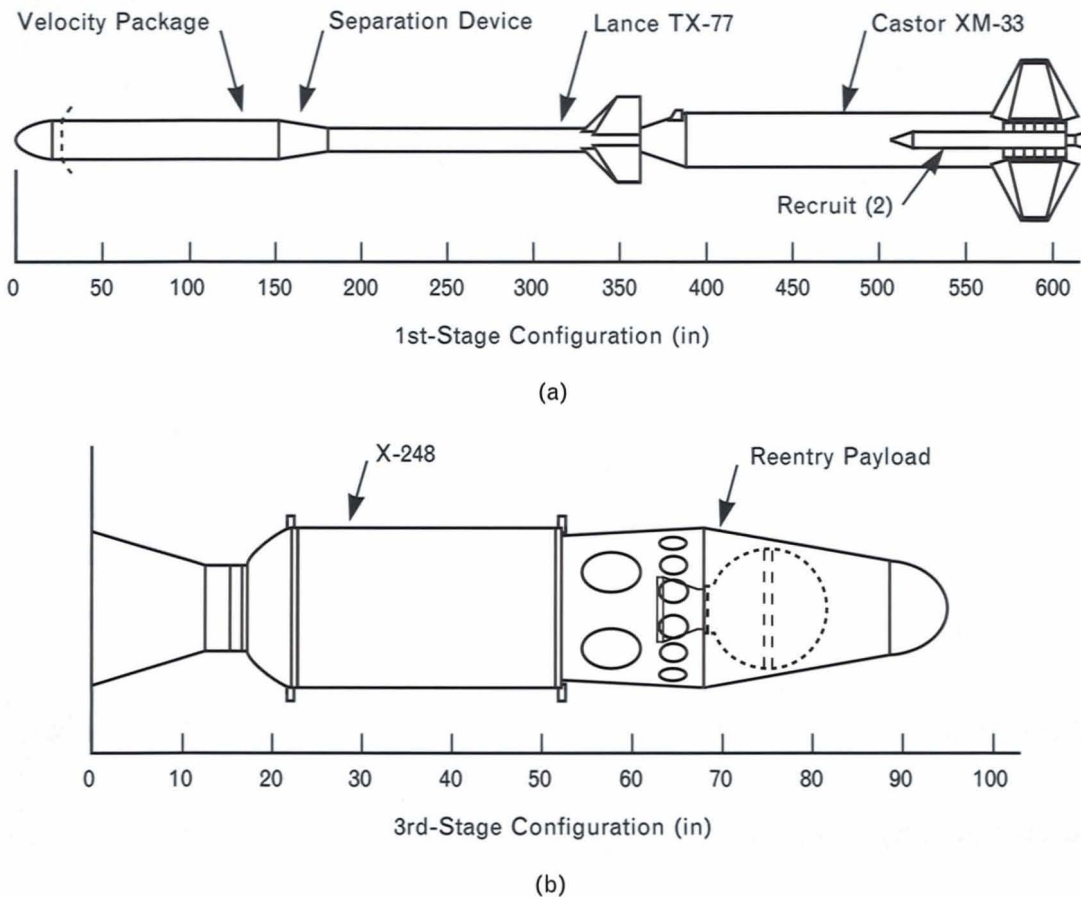


FIGURE 13. Trailblazer II reentry vehicle configuration. (a) The two up-firing stages of the launch vehicle consisted of Castor XM-33 and Lance TX-77 rockets; (b) the two down-firing stages consisted of an X-248 rocket and a reentry payload propelled by a 15-in spherical rocket motor.

Examination of the cross-polarized returns at UHF (i.e., the polarization orthogonal to the transmitted linear polarization) showed that a cross-polarized component started to appear shortly after initial wake onset. The orthogonal return was associated with the peak of the normal wake return and continued to grow until at the time of the peak wake return the orthogonal component was nearly equal to the normal return.

Artificial Meteors

For many years meteor astronomers had a strong interest in the determination of the total meteoric mass intercepted by the earth per unit time. The brightness and velocity of a natural meteor could be measured by existing chopped-track meteor cameras. The mass remained unknown, however, and the luminosity coefficient that

relates the deceleration and brightness of a meteor to its mass had yet to be determined. The creation and measurement of an artificial meteor of known mass was the only solution.

Trailblazer I reentry experiments routinely achieved last-stage reentry velocities of approximately 20,000 ft/sec. An additional down-firing stage capable of adding a velocity increment of 12,000 ft/sec to a pellet of approximately 2 g would place the reentry velocity of the pellet in the lower velocity range of natural meteors. Lincoln Laboratory joined Harvard Observatory, the Air Force Cambridge Research Laboratories (AFCRL), and NASA in an experiment to reenter a metallic pellet weighing approximately 2 g into the earth's atmosphere at a velocity of 32,000 ft/sec by using an explosive accelerator mounted on the front of a Trailblazer I sixth-stage 5-in spherical rocket motor. The explosive accelerator

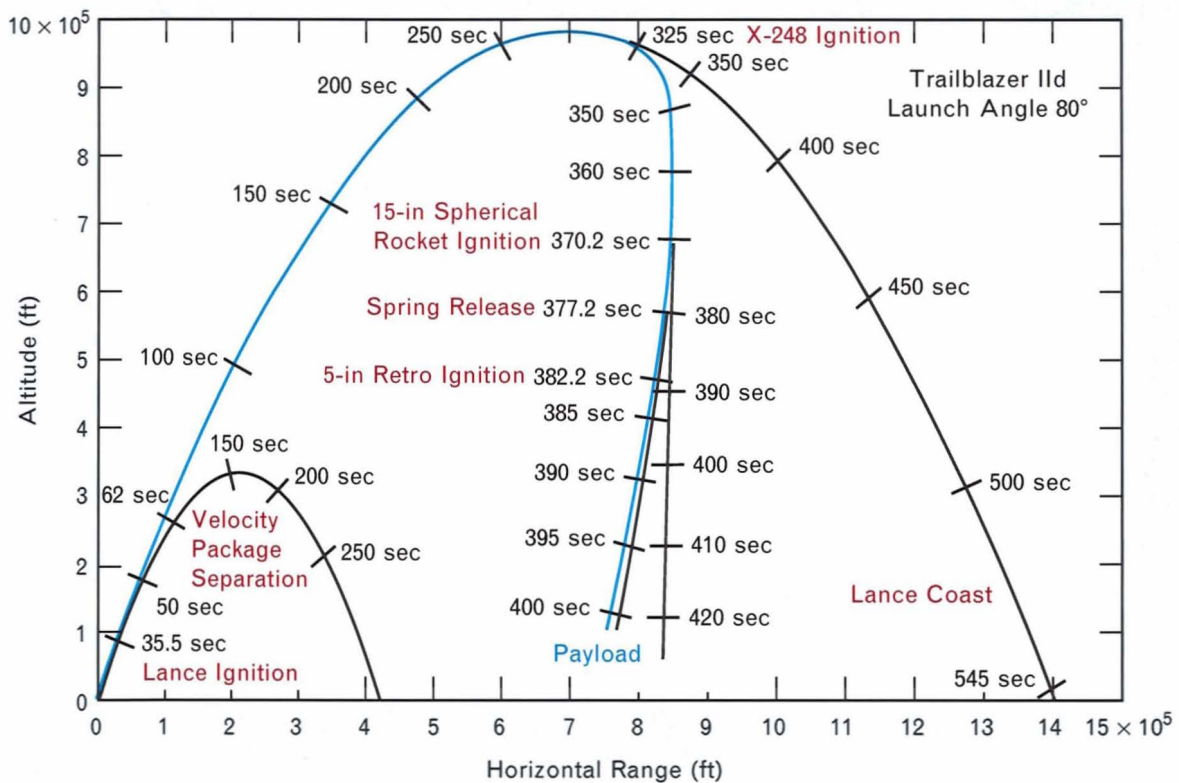


FIGURE 14. Typical Trailblazer II four-stage trajectories.

was developed by the University of Utah under contract to AFCRL. Figure 17 illustrates the explosive accelerator and the Trailblazer I sixth stage. On 21 April 1961, a Trailblazer I launch vehicle successfully reentered a 2-g pellet at a velocity of 32,000 ft/sec. The optical data from this experiment were used to make the first determination of the luminosity coefficient of natural meteors.

Because of the success of this experiment, we planned another artificial-meteor experiment using the larger Trailblazer II vehicle. In this second experiment, a 5-in spherical motor with an accelerator attached to its front surface was in turn mounted on the front of the 15-in fourth-stage rocket motor on a Trailblazer II launch vehicle. Figure 18 illustrates this launch vehicle configuration. Mounting the pellet accelerator on the front end of the 15-in reentry motor of the Trailblazer II increased the resulting pellet velocity by 15,000 ft/sec to approximately 47,000 ft/sec.

After the Lincoln Laboratory reentry measurements program terminated in 1965, NASA continued an ex-

panded artificial-meteor program at the Wallops Island launch facility. The small spectrographic Baby Schmidt camera was transferred by Lincoln Laboratory to NASA for use in that ongoing program.

Later Programs

During the course of the operation of the S-band tracking radar, starting in December 1959, returns were observed that were unrelated to any man-made target. These returns, which were assumed to be from natural objects, fell into two classes. The first class of returns exhibited negligible range extent and were usually amplitude modulated; the source of these returns were unknown at first but were later attributed to individual insects. The second class of returns were due to backscattering from index-of-refraction discontinuities in the atmosphere. This view was reinforced by the occasional appearance of horizontal layering in the returns. Because of the time pressures of the Reentry Physics Research Program, however, both the insect returns and the re-

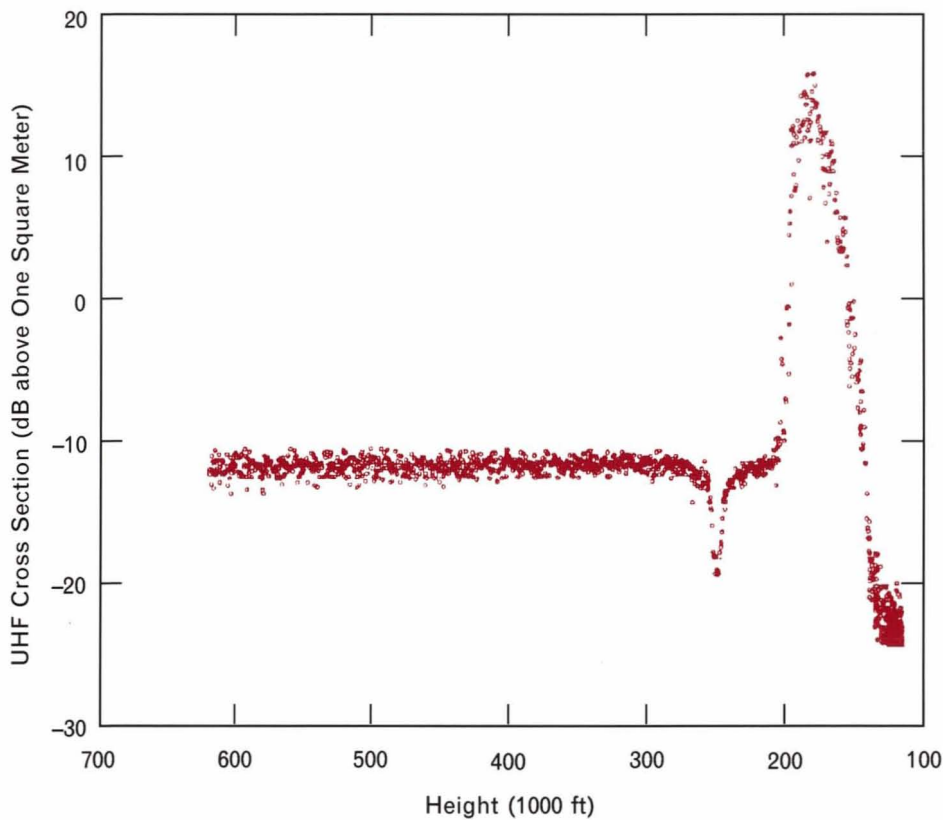


FIGURE 15. The UHF radar cross section versus altitude for the Trailblazer I spherical reentry body launched on 27 July 1962. This figure shows the typical cross-section dip at 250,000 ft. This dip occurs immediately prior to the large increase in cross section caused by the ionized wake behind the reentry body.

turns due to atmospheric discontinuities were not investigated further at that time.

Insect Returns

When the Lincoln Laboratory Reentry Physics Research Program was terminated in 1965, the tracking and measurement radars at Arbuckle Neck were transferred to NASA and the U.S. Air Force, and the facility became known as the Joint Air Force–NASA multiwavelength radar facility. The radars were then used to carry out a comprehensive series of measurements on the radar cross section of individual insects, and the amplitude and frequency of the cross-section variations due to their wing motion [2]. These experiments, performed in the summer of 1965, were a cooperative effort by AFCRL (which is now the Air Force Geophysics Laboratory), the Applied Physics Laboratory of Johns Hopkins University, and the Entomology Research Division of the U.S. Department of Agriculture.

In these experiments single insects in individual con-

tainers were carried aloft in a small aircraft that flew at an altitude above 1.5 km along a radial vector from the radar position (the vector coincided with the local wind direction). The S-band radar automatically angle-tracked the aircraft out to a range of approximately 10 km, at which point a single insect was released into the slipstream of the aircraft, auto tracking of the aircraft was discontinued, and the radar line of sight was frozen. After the return from the aircraft was sufficiently separated from that of the insect, automatic angle tracking was initiated on the insect. Hawkmoths, tobacco budworm moths, honeybees, and dragonflies were the subjects of these experiments. The S-band radar cross section of the hawkmoth, the dragonfly, and the honeybee was typically 10^{-3} cm². Measurements were also made at X-band, but no returns were observed with the UHF radar.

Radar observations of insects provided an answer to the mystery of *dot angels*, or echoes observed from otherwise invisible targets in the apparently clear atmosphere. Extensive research on dot angels showed that they were

indeed caused by insects in the air. These experiments also demonstrated that radar could be successfully used to measure entomologically significant parameters that had been considered essentially unmeasurable.

Atmospheric Variations in Index of Refraction

During the period of the reentry measurements program, we observed returns due to backscattering from discontinuities in the index of refraction in the atmosphere. These observations were made possible by the availability of the first high-powered S-band automatic tracking radar in which high performance was provided by the high sensitivity and low noise of the first operational liquid-N₂-cooled parametric amplifier, the high transmitter power of the radar, and the 60-ft antenna aperture.

From 1967 to 1971 the Weather Radar Branch of

AFCRL exploited the ability of these radars to obtain returns from atmospheric index of refraction variations in a major investigation of clear-air turbulence [3]. The radar observations were made simultaneously at all three frequencies, namely 400 MHz, 3 GHz, and 10 GHz, by scanning the antennas slowly in elevation while the video returns for each wavelength were displayed on separate range-height indicators whose screens were photographed for off-line analysis. These scans were performed at azimuths close to those for which the probe aircraft reported an encounter with significant turbulence. The probe aircraft were the F-100, F-4, F-84, F-86, and T-33. An RB-57 was also included because of its ability to operate at higher altitudes (up to 50,000 ft), and a C-130 was included because the effects of turbulence on that aircraft closely resembled the effects of turbulence on a commercial aircraft. Both the RB-57 and C-130 were able to

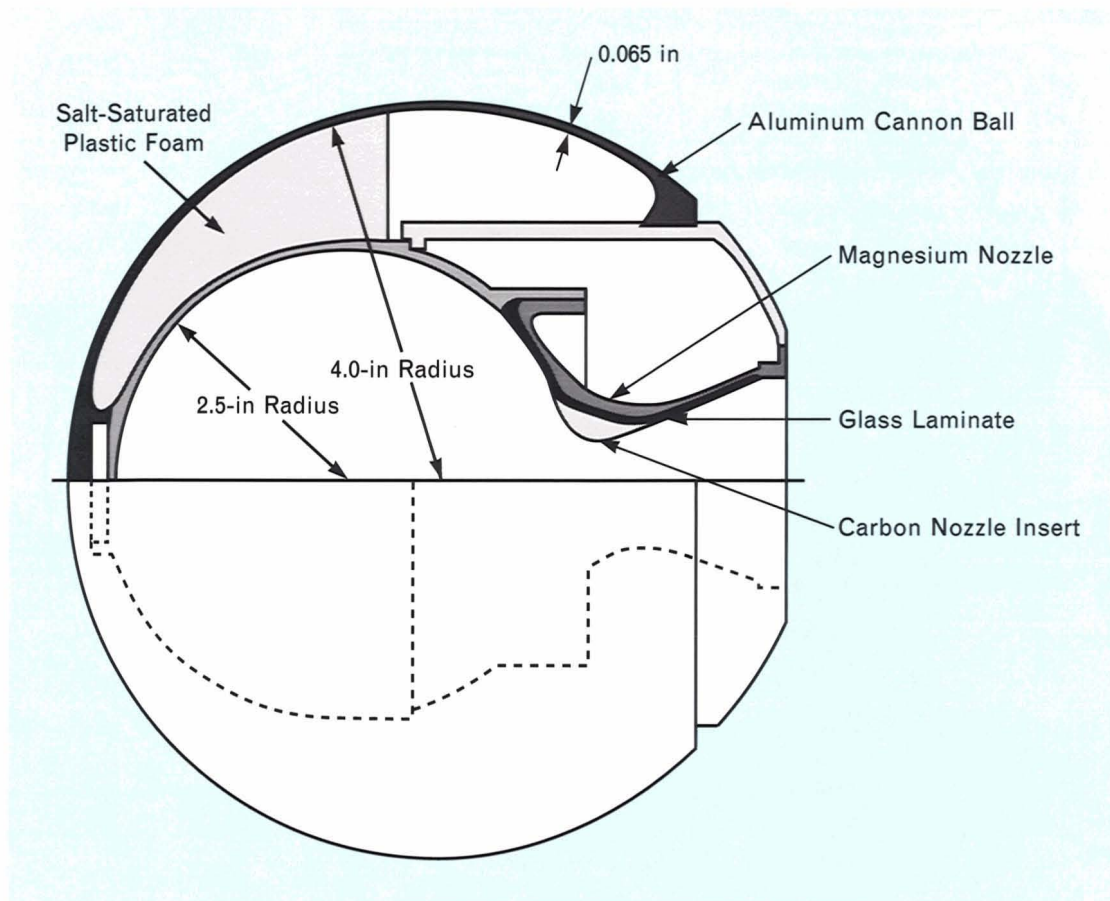


FIGURE 16. Configuration of the 8-in Trailblazer I spherical reentry body launched on 27 July 1962. The advantage of a spherical reentry body is that radar returns are independent of aspect angle, which makes the determination of cross section much easier.

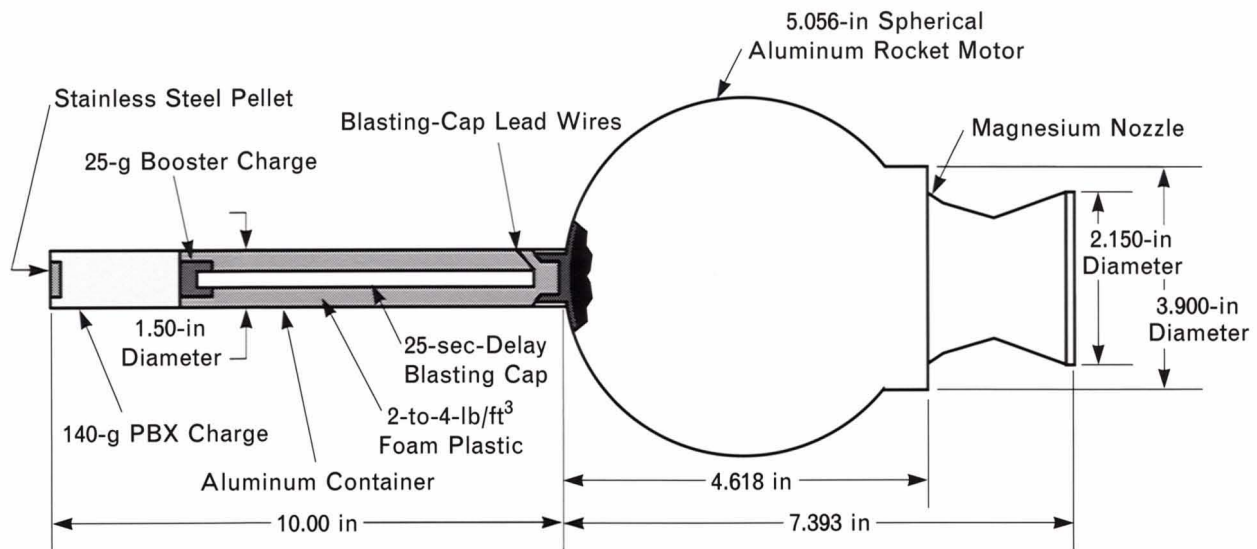


FIGURE 17. Sixth and seventh stages of the Trailblazer I vehicle used on 21 April 1961 to reenter the first artificial meteor at a velocity of 32,000 ft/sec. The seventh stage accelerated a 2-g pellet to a velocity close to that of natural meteors.

make longer atmospheric exploration flights. Meteorological data were also taken frequently during the radar measurements and aircraft flights.

Significant clear-air turbulence was observed during this program, and the usefulness of a powerful ground-based radar in the detection of clear-air turbulence was demonstrated. Today, building on the early research efforts at Wallops Island, the FAA has installed ground-based radars around the country to provide information and warning on clear-air turbulence to both commercial and military aircraft.

Acknowledgements

Daniel Dustin in the early 1950s recognized the nature of the ICBM threat, and along with Glen F. Pippert played a major role in the inception of the Reentry Physics Research Program at Lincoln Laboratory. This program, which was sponsored and supported by the Defense Advanced Research Projects Agency, ultimately involved many technical disciplines and crossed many organizational boundaries. Its success was due to the efforts and cooperation of a large number of dedicated

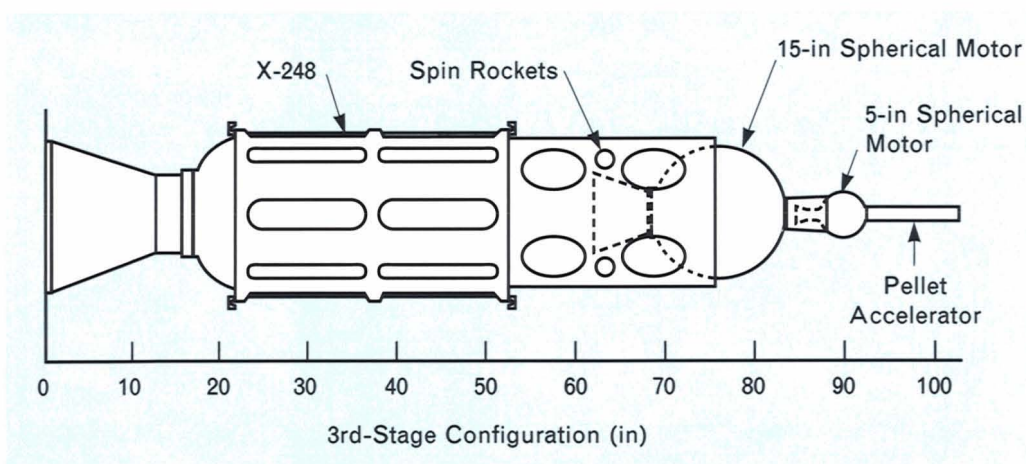


FIGURE 18. Third, fourth, and fifth stages of the Trailblazer II vehicle used to reenter an artificial meteor at approximately 47,000 ft/sec. This object combines the reentry stages illustrated in Figure 17 with the 15-in spherical motor of the Trailblazer II vehicle.

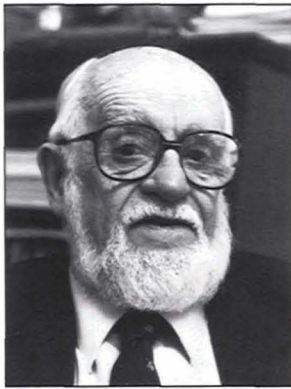
individuals whose contributions are gratefully acknowledged in alphabetical order as follows: Francisco L. Bacchialoni, Richard H. Baker, Edward Barsack, John R. Bauer, John Benvento, Edgar Blaisdell, Carl R. Bohne, Arthur E. Buckley, Ralph Burgess, James A. Daley, Crista de Ridder, Arthur C. Dyer III, Seymour Edelberg, Gabriel Farrell, Ovid V. Fortier, Claude L. Gillaspie, Eino O. Gronroos, Victor Guethlen, Paul Harris, John Howard, Frank Hutchinson, John Hutzenlaub, Kent R. Johnson, Harold L. Kasnitz, Robert H. Kingston, Kent Kresa, Kenneth E. Leathers, Vito N. Leone, James Marapoti, Robert Martinson, J.J. Mikulski, R.E. McMahon, Robert Meyer, John Paddleford, Edward Peters, Richard Peterson, Robert Pike, Lawrence J. Prugnarola, Hans W. Rudolph, James R. Sandison, George M. Shannon, Julius J. Sobolewski, Lawrence W. Swezey, Edward F. Tarbox, David Turck, John R. Williamson, Leo Wilber, P.A. Willmann, Frances A. Wilson, and Malcolm Woronoff.

In addition to the Lincoln Laboratory personnel list-

ed above, the following NASA personnel played major roles in the implementation of the Reentry Physics Research Program: Clarence Brown, R.T. Duffy, William N. Gardner, W.R. Hook, Reginald R. Lundstrom, and Ira W. Ramsey. Richard McCroskey, a member of the Harvard Observatory staff, was in charge of the Harvard effort centered on the Super Schmidt cameras.

REFERENCES

1. I.A. Getting, *All In a Lifetime—Science in the Defense of Democracy* (Vantage Press, New York, 1989).
2. K.M. Glover, K.R. Hardy, T.G. Konrad, W.N. Sullivan, and A.S. Michaels, "Radar Observations of Insects in Free Flight," *Science*, 154, 967 (25 Nov. 1966).
3. R.J. Boucher, "Evaluation of Clear Air Turbulence Detection by Ground-Based Radars, Special Rawinsondes, and Aircraft, 1967-1971," Air Force Cambridge Research Laboratories, Hanscom AFB, MA, 1 Oct. 1974.



LEO J. SULLIVAN is an associate group leader of the Laser Radar Measurements Group. He received an S.B. degree in physics from MIT in 1940. From 1942 to 1945 he was a staff member at the MIT Radiation Laboratory, where he worked on the development of automatic angle-tracking radar. This work led to the development of the SCR-584 gun-laying radar used by U.S. and British heavy antiaircraft batteries during the war. As a technical observer for the War Department, he received overseas assignments in England, North Africa, Italy, and France. In 1946 he joined the L.H. Terpening Co. in New York and designed radar components and systems. He joined the Johns Hopkins University Applied Physics Laboratory in 1948 and became Leader of the Tracking and Guidance Group that developed target-tracking and missile-guidance radars for the Terrier and Talos missiles. In 1953 he joined Lincoln Laboratory as a staff member in the Radar Division and worked on the development of pulsed Doppler radar. He later moved to the Radio Physics Division, where he designed an automatic tracking capability for the Millstone Hill microwave radar and its RF feed subsystem. In 1958 he began working in the area of reentry physics and its supporting microwave and optical instrumentation, including the design and construction of the multiwavelength radars and the 1.2-m

telescope installed at the Lincoln Laboratory field site at Arbuckle Neck, Va. He later participated in the design of the Project PRESS (Pacific Range Electromagnetic Signature Studies) reentry measurements system at the Kiernan Reentry Measurements Site (KREMS), located on Roi-Namur Island in the Marshall Islands group in the western Pacific. In 1967 he joined the Optics Division when it was formed and became involved in the laser radar effort at its inception. He continues to work in that area. In October 1990 he was presented with the first IRIS Active Systems Science and Technology Award for his lifetime contributions to the field of active systems.